Ab initio models of amorphous InN

B. Cai
Department of Physics and Astronomy, Ohio University, Athens, Ohio 45701, USA

D. A. Drabold
Department of Physics and Astronomy, Ohio University, Athens, Ohio 45701, USA
and Trinity College, Cambridge CB2 1TQ, United Kingdom
(Received 6 March 2009; published 8 May 2009)

In this paper, we present the first structural model of amorphous indium nitride obtained from first-principles simulation. We created a small 64-atom model by quenching from the melt and analyzed a chemically ordered 250-atom model of Mousseau and Barkema. We find that both N and In atoms tend to be fourfold. Upon relaxation, we find no homopolar bonds in the small cell and only one in the 250-atom cell. The topology of the models is analyzed with pair-correlation functions, bond angle distributions, and ring statistics. The vibrational and electronic properties are also obtained. We found that density-functional methods in the local-density approximation predict a very small gap for amorphous InN, similar to the case for crystalline InN.

DOI: 10.1103/PhysRevB.79.195204 PACS number(s): 61.43.Bn, 61.43.Dq, 63.50.Lm, 71.23.Cq

Amorphous materials and glasses play ever more important roles in technology. Due to photovoltaic, infrared detection and imaging applications, optoelectronic devices, and potential utility for next generation flash memory devices, the physics of amorphous semiconductors has drawn renewed interest. Since most properties of amorphous semiconductors are determined by topology, the beginning of any such study is the creation of experimentally credible structural model. A material of considerable current interest is the narrow gap semiconductor InN. Also, since GaN is an established wide-gap material, it is appealing to consider InGaN alloys for photovoltaic and other applications. Studies in this direction[1] would benefit from basic information about amorphous InN (a-InN). These materials might possess a continuously variable range of optical gaps to optimize absorption of the solar spectrum.[2]

There has been controversy over the band gap of zincblende crystalline-InN (c-InN) both in experimental and theoretical works. In experiment, a narrow band gap of 0.7 eV (Ref. 3 and 4) was reported, which contrasts with previous values near 1.89 eV.[5] Subsequently, these small gaps have been confirmed by additional experiments.[6–8] In theoretical work, calculations based on density-functional theory within the local-density approximation (LDA) always yield a tiny or even negative gap.[9] Methods using self-interaction and relaxation corrected pseudopotentials (SIRC) report a large gap around 1.3eV,[10] but semiempirical LDA methods show a gap around 0.85eV.[11] For amorphous InN (a-InN), a large optical gap around 1.7eV was measured in 2006.[12] However, no further experiments have been performed. No theoretical work has appeared on a-InN.

In this paper, we present atomic models of amorphous InN obtained from *ab initio* molecular dynamics based on plane-wave LDA. The structural, dynamical, and electronic properties are discussed. To our knowledge, there is neither theoretical nor experimental work on structural properties or vibrational modes. After creating small but reasonable models of a-InN, we *predict* the vibrational spectrum and electronic properties. We particularly seek to connect the electronic structure to the topology of the network to better comprehend electronic and optical experiments. We demonstrate by direct calculation that the topology of a-InN is a chemically ordered continuous random network very much along the lines proposed by Mousseau and Barkema.[13]

The simulations presented in our work are performed with the Vienna *Ab initio* simulation package (VASP) (Ref. 14) based on density-functional theory within the LDA and Vanderbilt's ultrasoft pseudopotentials.

To construct a realistic a-InN model, we began with the quench from the melt technique for a 64-atom model.[15] The initial configuration was melted at 2000 K and equilibrated for 800 steps. Then, the system is quenched to 400K, with a mean quench rate 61 K/ps. The system initially possesses a nitrogen dimer. According to Mott's eight-N rule and the electronegativity of these two elements, in theory, it is unlikely to form homopolar bond. Thus, we artificially moved this pair apart, then re-equilibrated the system at 400 K for 1000 steps (2.5 ps). Then the 64-atom a-InN model was relaxed to an energy minimum. During the MD procedure, the volume of the cell was constant. During the final relaxation, we allowed the volume and shape of the cell to change to ensure a zero-pressure model with no artificially imposed symmetries imposed on the shape of the cell. To check our small model, a 250-atom model was formed by relaxing an a-GaAs model[13] with Ga and As atoms replaced by In and N atoms, respectively. We rescaled the cell to reproduce the density of c-InN (also the density for 64-atom model) and relaxed the system at constant volume.

We present the topology of our final 64-atom model in Fig. 1. Because the shape of the cell is allowed to change during relaxation, the final cell is not quite cubic, but nearly so. The density of our final model is 6.97 g/cm^3 which is modestly larger than $6.81 \pm (0.05)$ g/cm^3, the density of c-InN. Where coordination is concerned, we note that all N atoms are fourfold and all but two In atoms are fourfold. There are no "wrong" (homopolar) bonds such as N-N or In-In in our model. It is gratifying to see chemical order emerge so unambiguously from an unbiased melt-quench procedure, a strong indication that homopolar bonds are rare in the material. For comparison, in the 250-atom model, we

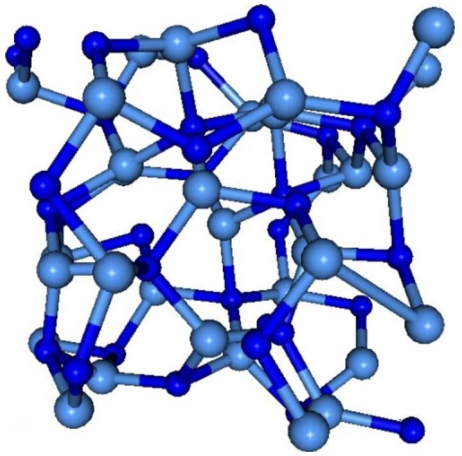

FIG. 1. (Color online) The structure of 64-atom model of a-InN. Blue (small sphere) represents nitrogen and gray (larger sphere) represents indium.

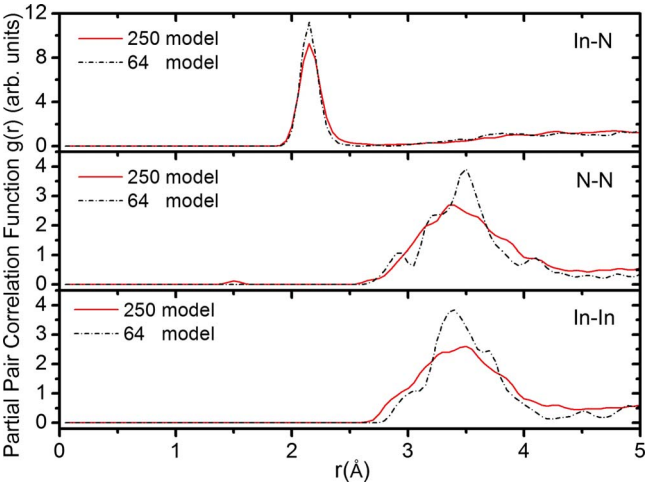

FIG. 2. (Color online) Partial pair-correlation functions of a-InN of 64-atom model (dashed line) and 250-atom model (solid line). From top to bottom: In-N, N-N, and In-In.

found that 87% N atoms are fourfold, 9% are threefold, and less than 4% are fivefold. Similarly, for In atoms, 88% are fourfold, 8% are threefold, and 4% are fivefold. Also there is one N-N bond in the 250-atom model, which could probably be eliminated if desired using the approach we employed for the 64-atom model. We summarize the results for the topology in Table I. The little increase in the under- and overcoordinated atoms in 250-atom cell could be attributed to the fact that the model is energetically relaxed while 64-atom cell is obtained through melt-quench technique, so the miscoordination could be just an artifact of the relaxation technique used. However, the apparent difference in coordination statistics is negligible in the sense that it did not cause any considerable change in the structural and electronic properties compared to the smaller 64-atom cell. Thus, we conclude that the 64-atom model and 250-atom model are consistent with each other.

We plot the pair-correlation functions of both models in Fig. 2. For 250-atom model, the small peak under 2 Å appearing in N-N plot is due to the homopolar bond mentioned before. For 64-model, the small peak and shoulder in N-N and In-In plots around 3 Å are due to the size effect. Besides that, the partial pair-correlation functions of both models are quite similar. There is a sharply defined peak at 2.15 Å for In-N. However, for N-N and In-In, the peak is broader and centered near 3.5 Å and 3.4 Å. Thus, the In-N pairs provide the dominant contribution to the first peak of total pair-correlation function. The N-N and In-In pairs provide the second peak of total pair-correlation function. To our knowledge, no experimental data are available, so this work is actually a *prediction*.

We also analyzed the angle distribution for In-N-In bonds and N-In-N bonds. The In-N-In angle has a mean value of 109.12°, which is close to the tetrahedral angle of 109.47°. The angle distribution shows the full width at half maximum (FWHM) is around 28°. The mean value of N-In-N bond angle is 108.78°, but the distribution is broader, with a FWHM around 34°. This result shows that nitrogen and indium atoms form tetrahedral units. However, there are some unexpected angles in our sample. We present the ring statistic result in Table II. From the table, we notice that there are no odd-membered rings in the network and this merely reiterates the absence of homopolar bonds. However, there are a few four-member rings. The existence of four-member rings implies that there are edge-sharing tetrahedra and other special units in our model which do not exist in c-InN. The situation is somewhat analogous to the case of a-SiO_2,[16] where the O-Si-O angles are tightly constrained near θ_T and the Si-O-Si angles have a broader distribution. We also computed the ring statistics in the 250-atom model. The results are also listed in Table II. Thus, from all of the data, we can conclude that 250-atom model has basically similar properties with 64-atom models. It is to be admitted that the 250-atom model is probably superior since strain effects are certain to be smaller in the larger supercell.

We describe the vibrational properties by analyzing the vibrational density of states (VDOS). In experiment, the VDOS can be obtained through inelastic neutron scattering, and information about the VDOS (modulated by hard-to-compute matrix elements) can be inferred from Raman measurements. In simulation, the vibrational energies are obtained from the dynamical matrix (matrix of the second derivatives of the energy with respect to the atomic positions). In VASP, the dynamical matrix (Hessian matrix) is determined by displacing each atom 0.015 Å in three or-

TABLE I. The statistical distribution of the main structural components in 64- and 250-atom models.

Model	N_3	N_4	N_5	In_2	In_3	In_4	In_5	n_N	n_{In}
64-atom	0	32(100%)	0	0	1(3.1%)	30(93.8%)	1(3.1%)	4	4
250-atom	11(8.8%)	109(87.2%)	5(4%)	1(0.8%)	10(8%)	110(88%)	4(3.2%)	3.95	3.94

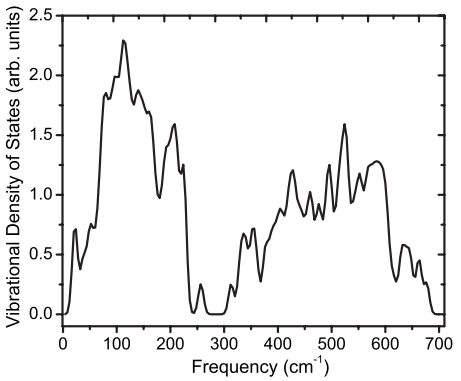

FIG. 3. Vibrational density of states of 64-atom model of amorphous InN. The vibrational eigenvalues were Gaussian broadened with a width of 7 cm^{-1}

thogonal directions. This yields the force-constant matrix from which the dynamical matrix is easily obtained.[17] Then the vibrational eigenvalues (the vibrational frequencies) are obtained by diagonalization. The density of states is obtained by Gaussian broadening of the eigenvalues. Figure 3 shows the vibrational state density of 64-atom model. There are two bands in VDOS. The lower (acoustic) band goes up to 240 cm^{-1} with two major peaks at 112 and 207 cm^{-1}. The higher-energy (optical) band is between 300 and 690 cm^{-1}.

The electronic properties of our models are analyzed through the electronic density of states (EDOS) and inverse participation ratio (IPR). The EDOSs are projected onto different atomic species and orbitals. We plot the detailed gap structure for both 64- and 250-atom models in Fig. 4. We found for both models that N atoms contribute more to valence tail but less to conduction tail relative to In. Second, the projections into *s*, *p*, and *d* channels show that the valence tail states are mostly associated with *p* electrons and the *d* electrons offer a larger contribution to the conduction-band tail. The importance of the projection into the *d* subspace emphasizes the need to include valence *d* states or polarization orbitals in a local-orbital representation.

For the 64-atom model, we found that the shape of the density of states (DOS) converges when more than 30 special **k** points are considered.[18] By considering only the Γ point, it appears that there is a small gap separating the valence and conduction bands. To correctly determine the position of ϵ_F and to ensure the convergence of our density of states, we repeated the analysis with various numbers of **k** points. ϵ_F shifts to the very top of the valence tail when sufficient **k** points are included. The results for 32 **k** points and 108 **k** points almost coincide, suggesting that DOS calculation is adequate for 32 points. For the 250-atom model, the calculation based only on Γ is enough to produce accurate EDOS. Similar to 64-atom model, a very small gap is observed. We accept the measured gap of ≈1.7 eV (Ref. 12) and suspect that our small gap largely has the same origin as the small LDA gap in c-InN, though the situation in the amorphous phase is more complex thanks to the formation of tails, especially at the conduction edge.

TABLE II. Ring statistics of a-InN. The number of *n*-member rings, $n=3$ through $n=7$.

Ring size	n_3	n_4	n_5	n_6	n_7
64-atom	0	30	0	320	0
250-atom	0	140	0	628	8

Thus, we conclude that for both models the Fermi level lies just at the top of valence tail which means there is at most a tiny gap. By carefully studying the difference between highest occupied molecular orbital (HOMO) and lowest unoccupied molecular orbital (LUMO) levels, we observed that the gap is smaller than 0.2 eV. This is not a surprising result since our density-functional approximations underestimate the gap and particularly so in InN in view of work on the topologically similar crystalline phases. Nevertheless, there is no reason to believe that the topology or dynamics should be critically affected by this, and furthermore, it is of interest to analyze the Kohn-Sham orbitals near the gap to gain insight into the defect states and levels.

In Fig. 5 we present the IPR plotted against energy for the 64-atom model. The IPR measures how localized (spatially compact) each state is. For a uniformly extended state, the value should be $\approx 1/N$, here $N=64$, the number should be 0.016. For an ideally localized state, the IPR value should be close to unity. From Fig. 5, we observe that the IPR is never large, which indicates the localization of those states is not very high. However, there are some weakly localized states on the tail. The results are confirmed by IPR analysis for 250-atom model: IPR there is commensurately small and valence and conduction-band tail have a few somewhat localized states.

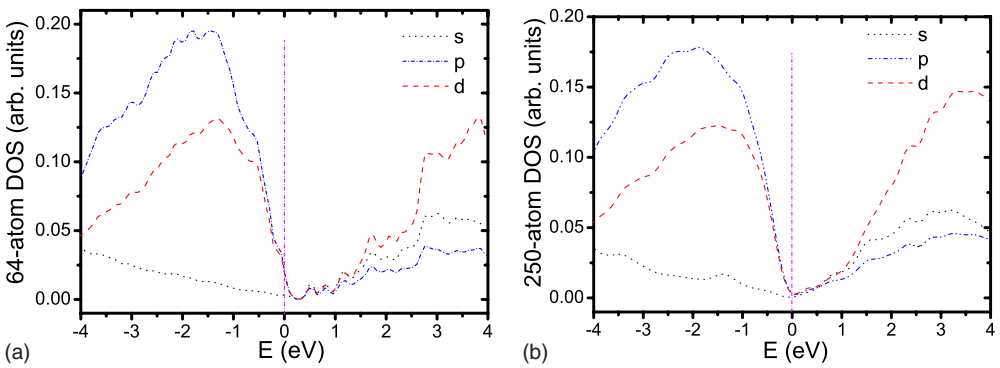

FIG. 4. (Color online) Detailed gap structure for 64- and 250-atom models. Vertical line indicates the position of Fermi level, ϵ_F.

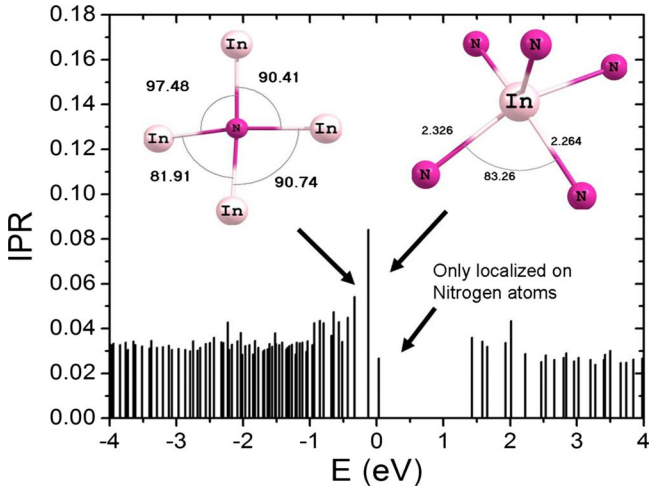

FIG. 5. (Color online) IPR for different states near the optical gap and special units upon which the states are localized (see text).

If we project the IPR onto different atoms, we determine the specific atoms on which a selected state is localized. We observed for the 64-atom model that one valence tail state was localized on an N atom which formed four angles near 90°. Another valence tail state was localized on two N atoms which are the fourth and fifth neighbors of the only fivefold In atom (also with longer bond lengths larger than typical). Also the gap states are preferentially localized on N atoms and less so onto In atoms.

Finally, to understand the electronic signature of defects in the amorphous phase, we performed the calculation on models with defects such as vacancies, antisite defects, and wrong bonds. We only consider single defect in each case. For example, for vacancy, we take one atom out of the system; for antisite defect, we replace one N (or In) atom with In (or N) but do *not* relax the system. When single N vacancy is introduced, ϵ_F shifts toward the conduction edge and additional conduction tail states which are localized on the neighbors of that N vacancy are pushed into the gap. Similar to N vacancy, highly localized conduction-band tail states are induced by the N antisite defect. But the shift in ϵ_F is small compared to N vacancy and toward conduction band. Since Fermi level shifts toward conduction band, these two kinds of defects make the semiconductor *n* type. On the contrary, a remarkable movement of ϵ_F toward valence-band tail is observed in the presence of an In vacancy. The In antisite defect also slightly shifts ϵ_F to the valance tail. In both case, highly localized valance band tail states are observed which correspondingly associate with neighbors of In vacancies and In antisite defect. Thus, these two kinds of defects may make the system *p* type. Finally, for N-N "wrong" bond, it produces both valence tail states and conduction states. The Fermi level is shifted into gap.

We have discussed the topology, vibrational dynamics, and electronic structure of amorphous InN. The topology of this material is found to be tetrahedral and chemically ordered. We hope our model will provide a helpful starting point for future work.

We gratefully acknowledge the National Science Foundation for support under Grant No. DMR-0600073 and the Army Research Office and Army Research Laboratory under Cooperative Agreement No. W911NF-0-2-0026. D.A.D. thanks the Leverhulme Trust (U.K.) and the NSF International Materials Institute for New Functionalities in Glass for supporting work undertaken at the University of Cambridge. We particularly thank N. Mousseau and G. Barkema for sending us the coordinates of their highly realistic 250-atom model of a-GaAs that we converted by computer alchemy to a-InN. We are grateful to Mingliang Zhang and Fakhar Inam for helpful discussion. We thank M. Kordesch and D. Hoy for many suggestions and indeed for providing the original motivation for undertaking this work.

[1] For example, S. J. Lee, Jpn. J. Appl. Phys., Part 1 **37**, 5990 (1998); X. Zhang, S.-J. Chua, W. Liu, and P. Li, Phys. Status Solidi B **216**, 307 (1999).
[2] J. Wu, W. Walukiewicz, W. Shan, K. M. Yu, J. W. Ager, E. E. Haller, H. Lu, and W. J. Schaff, Phys. Rev. B **66**, 201403(R) (2002).
[3] J. Wu, W. Walukiewicz, K. M. Yu, J. W. Ager, E. E. Haller, H. Lu, W. Schaff, Y. Saito, and Y. Nanishi, Appl. Phys. Lett. **80**, 3967 (2002).
[4] V. Yu. Davydov, A. A. Klochikhin, V. V. Emtsev, S. V. Ivanov, V. V. Vekshin, F. Bechstedt, J. Furthmuller, H. Harima, A. V. Mudryi, A. Hashimoto, A. Yamamoto, A. J. Aderhold, J. Graul, and E. E. Haller, Phys. Status Solidi B **230**, R4 (2002).
[5] T. L. Tansley and C. P. Foley, J. Appl. Phys. **59**, 3241 (1986).
[6] M. Higashiwaki and T. Matsui, J. Cryst. Growth **269**, 162 (2004).
[7] D. B. Haddad, H. Dai, R. Naik, C. Morgan, V. M. Naik, J. S. Thakur, G. W. Auner, L. E. Wenger, H. Lu, W. J. Schaff, Mater. Res. Soc. Symp. Proc. **798**, Y12.7.1-6 (2004).
[8] K. S. A. Butcher and T. L. Tansley, Superlattices Microstruct. **38**, 1 (2005).
[9] J. Deng, F. Ye, Q. Y. Long, and C. W. Lung, Phys. Rev. B **59**, 8 (1999).
[10] J. Juraszek, A. Fnidiki, J. Teillet, M. Toulemonde, A. Michel, and W. Keune, Phys. Rev. B **61**, 12 (2000).
[11] S.-H. Wei, X. Nie, I. G. Batyrev, and S. B. Zhang, Phys. Rev. B **67**, 165209 (2003).
[12] J. M. Khoshman and M. E. Kordesch, J. Non-Cryst. Solids **352**, 5572 (2006).
[13] N. Mousseau and G. T. Barkema, J. Phys.: Condens. Matter **16**, S5183 (2004).
[14] G. Kresse and J. Furthmuller, VASP the guide 2003, http://cms.mpi.univie.ac.at/vasp/
[15] For an extended discussion, see D. A. Drabold, Eur. Phys. J. B **68**, 1 (2009).
[16] De Nyago Tafen and D. A. Drabold, Phys. Rev. B **71**, 054206 (2005).
[17] P. Ordejon, D. A. Drabold, R. M. Martin, and S. Itoh, Phys. Rev. Lett. **75**, 1324 (1995).
[18] H. J. Monkhorst and J. D. Pack, Phys. Rev. B **13**, 5188 (1976).